# Making closed-shell lead phthalocyanine paramagnetic on Pb(100)

Jan Homberg, Alexander Weismann,* and Richard Berndt†
*Institut für Experimentelle und Angewandte Physik, Christian-Albrechts-Universität zu Kiel, D-24098 Kiel, Germany*

(Received 13 February 2024; revised 28 March 2024; accepted 29 March 2024; published 16 April 2024; corrected 2 May 2024)

Lead phthalocyanine (PbPc), a nonplanar molecule, is studied on Pb(100) by scanning tunneling spectroscopy. A rigid shift of the molecular orbitals is found between molecules with the central Pb ion pointing toward (PbPc ↓) or away from (PbPc ↑) the substrate and is understood from the interaction between the molecules and their image charges. Within the superconducting energy gap, Yu-Shiba-Rusinov (YSR) resonances are observed for PbPc ↑ molecules in islands, indicating the presence of a magnetic moment. Such bound states are not present on PbPc ↓ molecules, nor on isolated PbPc ↑ or molecules that have lost the Pb ion during deposition ($H_0$Pc). The YSR energies vary depending on the orientation and type of the molecular neighbors. We analyze the role of the out-of-plane electrostatic dipole moment of PbPc.

DOI: 10.1103/PhysRevB.109.165426

## I. INTRODUCTION

Molecular spintronic devices at the limit of miniaturization involve magnetic complexes in contact with conducting electrodes [1]. However, the close proximity of a substrate can interfere with molecular functions through electronic and steric interactions and can lead to fragmentation [2,3]. On the other hand, the effect of a substrate can be more favorable. For example, different spin states resulting from charge transfer have been reported from metal-free porphyrin on Au(111) [4] and from aza-triangulene molecules on the (111) surfaces of Ag and Au [5]. Spin-state switching of closed-shell retinoic acid was observed on Au(111) and interpreted as a sigmatropic reaction [6,7]. The importance of the molecule-substrate interactions for the spin-crossover effect was repeatedly highlighted [8–13]. The diamagnetic closed-shell molecule phthalocyanine ($H_2$Pc) and aluminum phthalocyanine (AlPc) have been found to become paramagnetic on a Pb substrate [14,15]. This striking effect was attributed to electrostatic interactions in molecular arrays and was not observed from isolated adsorbed molecules. Tuning of the intermolecular interactions can therefore be used to control molecular magnetism in the latter cases.

The tool used to probe the magnetism of individual phthalocyanine molecules is scanning tunneling spectroscopy of Yu-Shiba-Rusinov (YSR) resonances [16–18]. These resonances arise from the interaction of a magnetic impurity with the Cooper pairs of a superconductor and appear as prominent peak pairs at energies $\pm E_{\mathrm{YSR}}$ in the excitation gap of the superconductor. This effect has been studied for magnetic atoms and molecules [10,19–32], in part as a platform for the construction of systems that support Majorana modes [33–36].

So far, $H_2$Pc and AlPc have been discovered to acquire a spin under the influence of suitably arranged nearest neighbors. Both molecules are planar and exhibit charge imbalances in the molecular plane. Here we report on nonplanar lead phthalocyanine (PbPc). This complex exhibits a vertical electrostatic dipole moment that is known to have implications for the electronic states of the system [37–40]. Similar to tin phthalocyanine (SnPc) on Ag(111) [41–45], PbPc can be adsorbed on Pb(100) with the central ion pointing to (PbPc ↓) or away (PbPc ↑) from the substrate. We observe a rigid shift of the molecular orbitals between these orientations. We also find YSR resonances, but only for PbPc ↑ molecules embedded in dense arrays. Variations of the YSR energies with the orientations and types of the molecular neighbors are explored experimentally.

The article is structured as follows. After a brief description of the experimental procedures, we first present aspects of the geometrical structure of PbPc on Pb(100). The nonplanar shape of the molecule and the possibility of demetallization add a certain complexity to the observed structures. Next, data on the molecular electronic states are presented and discussed. We first consider the frontier orbitals and the molecular charge distribution. Then the YSR resonances, which signal paramagnetism, are analyzed in detail. We emphasize that the YSR energies and the spectral shapes scatter over a wide range and show that this variability can be explained by the structural properties and electrostatic considerations.

## II. EXPERIMENTAL METHODS

Experiments were performed with two scanning tunneling microscopes operated in ultrahigh vacuum (UNISOKU USM-1300 and a homebuilt instrument). Sample temperatures between 1.6 and 4.2 K were used. Pb(100) single crystals were prepared by Ar-ion sputtering and annealing to approximately 230 °C. Scanning tunneling microscopy (STM) tips were cut from a Pb wire and sputtered in ultrahigh vacuum. Submonolayer coverages of PbPc molecules were deposited

*weismann@physik.uni-kiel.de
†berndt@physik.uni-kiel.de

 

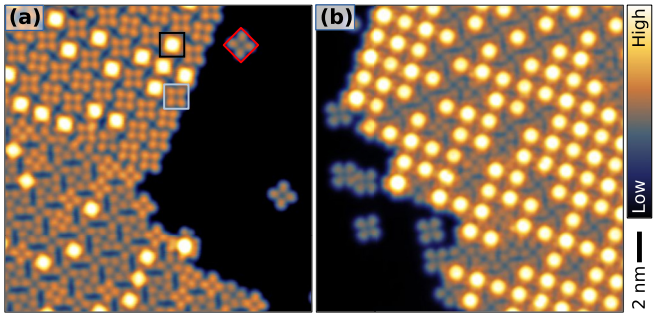


FIG. 1. Topographs of submonolayer coverages of PbPc on Pb(100). (a), (b) Images from two separate experimental runs. The PbPc molecules assemble into ordered islands. In addition, isolated $H_0$Pc molecules are found. Squares in black, light blue, and red indicate examples of PbPc ↑, PbPc ↓, and $H_0$Pc molecules, respectively. In the upper-left and lower-left parts of (a), two molecular domains are discernible. Imaging parameters: (a) $I = 200\,\text{pA}$, $V = -10\,\text{mV}$; (b) $I = 100\,\text{pA}$, $V = 100\,\text{mV}$.

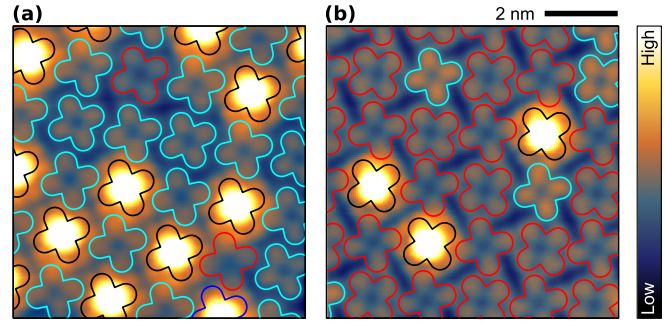


FIG. 2. Topographs with molecular outlines indicated. (a), (b) Domains A and B. Black, light blue, and red lines show PbPc ↑, PbPc ↓, and $H_0$Pc molecules. In domain A, the orientations of all molecules are fairly similar, while nearest neighbors are rotated by $\approx 20^\circ$ with respect to each other in domain B. Imaging parameters: $I = 100\,\text{pA}$, $V = 6\,\text{mV}$ in (a) and $-6\,\text{mV}$ in (b).

from a Knudsen cell onto the Pb surface, which was close to ambient temperature.

## III. GEOMETRIC STRUCTURE

### A. Observed types of molecules

After the deposition of submonolayer amounts of PbPc we found molecules in a number of structures, namely, isolated molecules, regular arrays of molecule-covered steps, and molecular islands. We observed three main types of molecules (Fig. 1). Intact molecules are adsorbed with their Pb ion pointing to the vacuum side (PbPc ↑, black square) or to the substrate (PbPc ↓, light blue square), as previously observed from nonplanar SnPc [44]. In addition, some molecules have lost the central Pb ion and are denoted $H_0$Pc (red square) below.

While PbPc ↑ molecules are easily recognized by their protruding Pb atom, the differences between PbPc ↓ and $H_0$Pc molecules are more subtle, with PbPc ↓ molecules appearing slightly higher than $H_0$Pc. For the identification of $H_0$Pc, we used manipulations with the STM tip. At elevated currents PbPc ↑ can be demetallized like SnPc [46], leaving behind $H_0$Pc. Alternatively, we prepared $H_0$Pc by removing the central H atoms from $H_2$Pc [47]. In both cases the images of the remaining $H_0$Pc are identical to those of the molecules identified as $H_0$Pc after PbPc deposition. Furthermore, $H_0$Pc molecules were reproducibly converted to PbPc ↑ by transferring atoms from the Pb tip, which was not possible on PbPc ↓ molecules. In addition to the differences in constant current images, the three types of molecules exhibit different conductance spectra as detailed below.

In Fig. 1(a), the fraction of PbPc ↑ molecules is lower than in (b). In fact, we observed different fractions of PbPc ↑, PbPc ↓, and $H_0$Pc molecules in repeated experimental runs, presumably due to different substrate temperatures during deposition.

We note in passing that $H_0$Pc molecules were often isolated rather than embedded in islands. This observation suggests reduced diffusion of the $H_0$Pc radical that may be due to chemisorption, whereas PbPc is expected to be physisorbed like, e.g., Cu-phthalocyanine [48]. In addition, we have verified that $H_0$Pc molecules can be converted to $H_2$Pc by introducing hydrogen from the STM tip, as previously demonstrated on Ag(111) [47].

### B. Structure of ordered islands

In ordered islands [see, for example, Fig. 1(a)] we often observed two types of domains. Close-up views of these domains are displayed in Fig. 2 along with outlines indicating the molecular arrangement. Schematic representations of the molecular geometries and the substrate lattice are shown in Fig. 3(a), which shows a checkerboard pattern with two molecules per unit cell, similar to the case of $H_2$Pc [14]. In each domain the two molecules have different orientations with respect to the underlying Pb(100) lattice, resulting in a total of four orientations [Fig. 3(b)]. In domain A, the angles to a ⟨110⟩ direction of the substrate are 46° (A1) and 54° (A2). In domain B they are 21° (B1) and 1° (B2). These values are based on an analysis of more than 125 molecules, which led to the histogram in Fig. 3(c). The patterns of the domains closely resemble geometries made from $H_2$Pc on Pb(100) [14].

## IV. ELECTRONIC STRUCTURE

### A. Spectroscopy of molecular orbitals

Figure 4 shows the $dI/dV$ spectra of PbPc ↑, PbPc ↓, and $H_0$Pc molecules in a type-A island. The measurements were performed at constant current to allow spectroscopy over a wide voltage range. This technique also tends to sharpen and slightly downshift spectral peaks compared to constant-height spectroscopy [49]. Multiple resonances are observed, which we attribute to molecular orbitals. The lowest unoccupied molecular orbital (LUMO) of PbPc ↑ in the islands is very close to $E_F$ and is not included in the corresponding spectrum. PbPc ↓ and $H_0$Pc [Figs. 4(b) and 4(c)] exhibit LUMO resonances near 300 and 180 mV, respectively. We use this difference to distinguish between these molecules despite their similar image contrast. Three other peaks are observed from all molecules and are assigned to the LUMO + 1

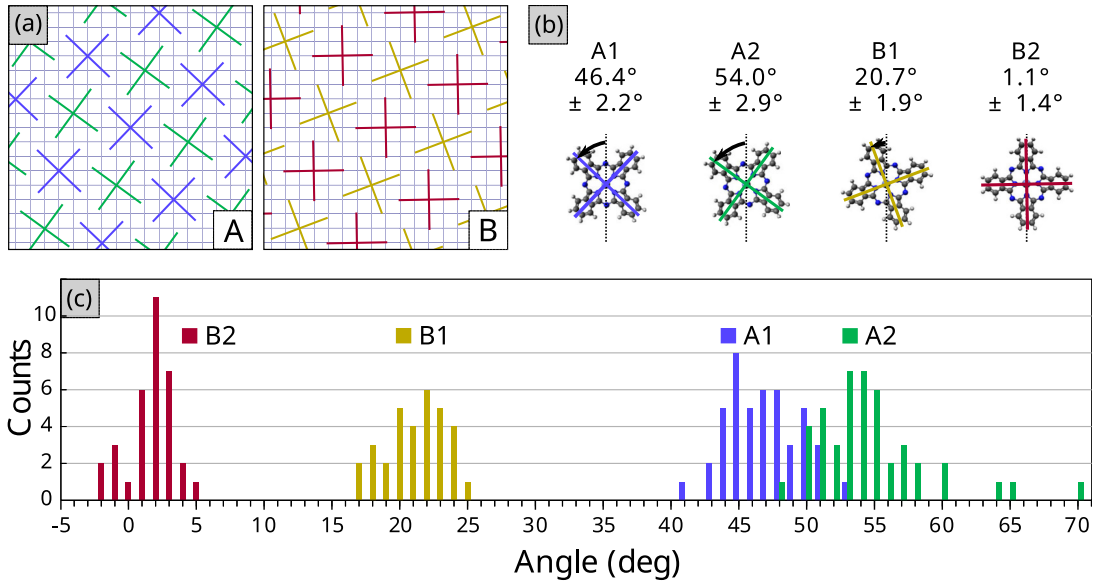


FIG. 3. Adsorption geometry of PbPc on Pb(100). (a) Models of domains A and B. The square Pb(100) mesh is indicated by gray lines. Phthalocyanine molecules with different orientations are displayed as colored crosses. The molecules are arranged in a $\begin{bmatrix} 5 & 3 \\ -3 & 5 \end{bmatrix}$ superstructure with two molecules per unit cell and occupy atop positions. (b) Molecular models of the orientations, which are described by the angles (arrows) enclosed between a molecular lobe and a ⟨110⟩ direction. (c) Histogram of observed angles from 32 B1, 33 B2, 45 A1, and 45 A2 molecules. The scatter is partially due to measurement uncertainty ($\approx \pm 2^\circ$). In a few cases, e.g., $>60^\circ$, the molecular orientation does not fall in any of the four classes.

to LUMO + 3. The peak at $V < 0$ for PbPc ↑ may represent the highest occupied molecular orbital (HOMO) of this molecule. The weakness of this signal and the absence from the other spectra can be understood from the lateral distribution of the HOMO of phthalocyanines, which vanishes at the molecular center [50–52]. In addition, features at positive sample voltage are usually more intense in tunneling spectroscopy [53,54].

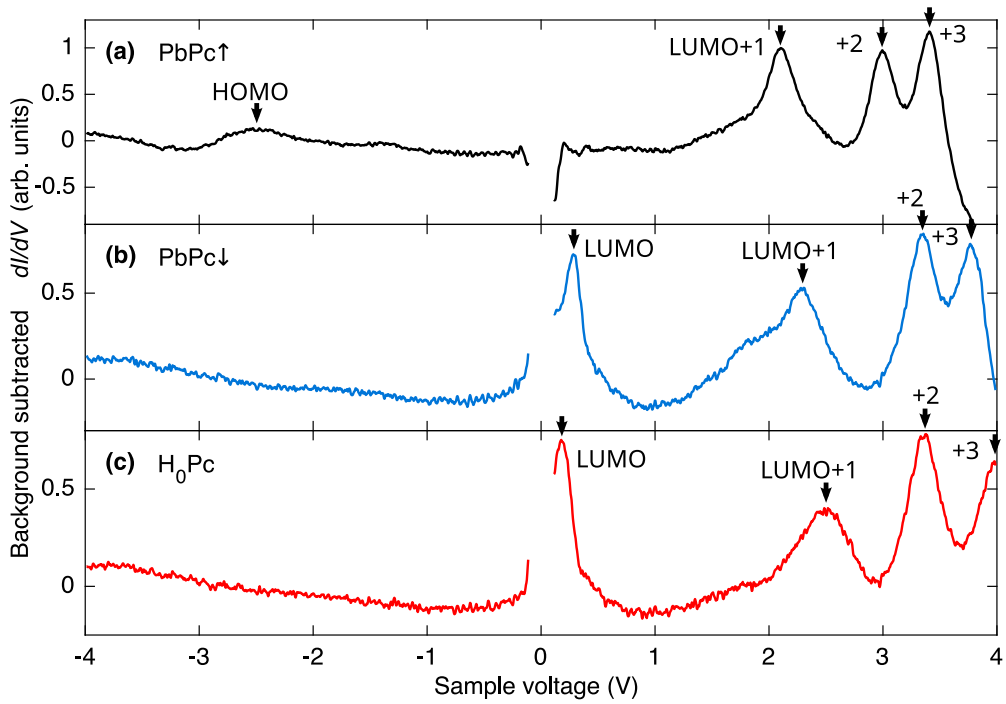


FIG. 4. $dI/dV$ spectra measured at constant $I = 76$ pA with the tip placed above (a) PbPc ↑, (b) PbPc ↓, and (c) $H_0$Pc molecules inside a domain-A island. Data at positive and negative $V$ were measured separately, starting at $V = \pm 100$ mV. A voltage modulation $V_M = 14.1$ $mV_{PP}$ was used. A reference spectrum taken on the Pb(100) substrate has been subtracted from each data set. Arrows indicate major resonances that we attribute to molecular orbitals.

TABLE I. Energies of the molecular orbitals from spectra of Fig. 4 in electronvolts relative to $E_F$. The LUMO of PbPc ↑ is close to $E_F$ and is not discernible in Fig. 4(a).

| Orbital | PbPc ↑ | PbPc ↓ | $H_0$Pc |
|---|---|---|---|
| LUMO+3 | 3.4 | 3.8 | ⩾4.0 |
| LUMO+2 | 3.0 | 3.3 | 3.4 |
| LUMO+1 | 2.1 | 2.3 | 2.5 |
| LUMO | ≈0 | 0.3 | 0.2 |
| HOMO | −2.5 | | |

The measured peak energies of the unoccupied orbitals of the three molecules are arranged in rather similar patterns (Table I). The LUMO + 1 is separated by ≈1 eV from the LUMO + 2, which in turn lies ≈ 0.5 eV lower than the LUMO + 3. The PbPc ↑ orbitals are shifted down by ≈ 0.3 eV with respect to PbPc ↓. As will be detailed below, this can be understood qualitatively from the molecular electrostatic dipole. The energy shift is crucial for the appearance of YSR states on PbPc ↑ molecules because it leads to a partial occupation of the LUMO.

To quantify the electrostatic stray field of PbPc and its influence on the orbital energies, gas-phase density-functional theory (DFT) calculations were performed. The atoms of the Pc framework were constrained to one plane during structure optimization, while the Pb atom was allowed to relax in all three directions. A Mulliken population analysis revealed negative partial charges of ≈0.2 e on the nitrogen atoms and finds Pb and macrocyclic carbon atoms to be positively charged by ≈ 0.25 and 0.13 e, respectively. Peripheral C-H bonds are found to be polar with positive (negative) partial charges of ≈ 0.08 e (≈ 0.06 e) on the H (C) atoms. Figure 5 shows the calculated image potential $V_{im}(\mathbf{x})$ of PbPc ↑ and PbPc ↓ molecules. We used the molecule-substrate distances previously determined from DFT calculations that included the substrate [30] and placed the image plane 100 pm above

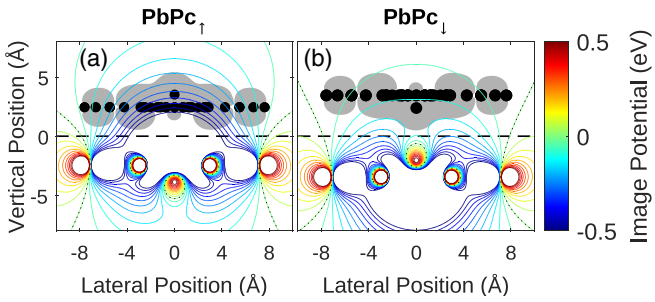


FIG. 5. Image potential of (a) PbPc ↑ and (b) PbPc ↓ molecules calculated from the Mulliken charges from gas-phase DFT calculations. The image plane used is indicated by a dashed line. The molecules are represented by black dots at the projected atomic positions and a gray area representing constant LUMO density. Colored contour lines range from – 500 (blue) to 500 meV (red) in increments of 50 meV. $V_{im} = 0$ is further marked using black dotted lines. Negatively charged nitrogen atoms of the molecular macrocycle are accompanied by positive image charges that lower the LUMO energy. For PbPc ↓, the downshift is largely compensated by the negative image charge of the central Pb ion.

the topmost substrate nuclei. The electrostatic shifts of the unoccupied DFT wave functions $\Psi_i$ were evaluated using $\int d^3\mathrm{x}|\Psi_i(\mathbf{x})|^2 V_{im}(\mathbf{x})$. We find a decrease of the energies for PbPc ↑ and PbPc ↓ molecules of approximately –300 and –80 meV, respectively. The difference between these values matches the experimental shift between the PbPc ↑ and PbPc ↓ states (300 meV) rather well. The downshifts are caused by the net positive image charge of the C and N atoms of the Pc macrocycle (0.6 e in total). The negative image charge of the positive Pb atom partially compensates for the downshift, which is the main reason for the different results for PbPc ↑ and PbPc ↓.

### B. Spectroscopy of YSR states

In the following we focus on PbPc ↑ molecules in islands because they exhibit spectral features close to the Fermi energy $E_F$ that are consistent with YSR resonances. Isolated PbPc ↑ molecules do not exhibit such features. Neither do PbPc ↓ or $H_0$Pc molecules, regardless of their environment.

Figure 6 shows the corresponding conductance spectra of PbPc ↑ molecules, either isolated (blue) or in an island (red). The overview spectra in panel (a) reveal that the LUMO energy of PbPc ↑ is lowered by ≈100 meV when the molecule is surrounded by neighbors. This LUMO shift is accompanied by a drastic change in the low-energy excitations [Fig. 6(c)]. While the spectrum of the isolated molecule (blue) is essentially a copy of the substrate spectrum (not shown), the molecule with neighbors shows YSR peaks near ±2 mV. The lateral distributions of the LUMO [Fig. 6(b)] and the YSR states [Fig. 6(d)] are similar. The intensity is highest in a ring-shaped area above the Pb ion, and some intensity is found on the macrocycle and the lobes. This distribution can be understood from the LUMO of PbPc as calculated with density functional theory [50]. The LUMO is doubly degenerate and includes hybridized $p_x$ and $p_y$ orbitals of the Pb ion, which in combination give rise to the ring shape. The spectroscopic data closely resemble earlier observations from $H_2$Pc [14] and suggest that the YSR state is supported by the LUMO.

Despite the spectroscopic similarities between $H_2$Pc and PbPc, there are also differences. First, the YSR energies of PbPc cover a wider range, starting from $E_{\mathrm{YSR}} \approx \Delta$ down to ≈ 0.4Δ, where $\Delta = 1/2(\Delta_T + \Delta_S) = 1.33$ meV is the average superconducting gap parameter of the tip and sample [55]. For $H_2$Pc, the energies were restricted to $E_{\mathrm{YSR}} \gtrsim 0.9\Delta$. Second, the variation of $E_{\mathrm{YSR}}$ on $H_2$Pc was interpreted in terms of the tautomeric configurations and the associated quadrupole moments of the neighboring molecules. However, PbPc does not have a quadrupole moment, and consequently, the shifts of $E_{\mathrm{YSR}}$ must have a different origin.

#### *Variation of YSR energies.*

$dI/dV$ spectra were measured for hundreds of PbPc ↑ molecules. Characteristic data are shown in Fig. 7. Resolving the YSR and coherence peaks as clearly separated features is only possible when $E_{\mathrm{YSR}} \ll \Delta$, e.g., in Fig. 7(e). To deal with spectra with overlapping peaks, we define a reduced peak energy $\tilde{E}_P = eV_P/\Delta - 1$. Without a YSR state $\tilde{E}_P = 1$, and with a pronounced YSR state $\tilde{E}_P \approx \tilde{E}_{\mathrm{YSR}} = E_{\mathrm{YSR}}/\Delta$. A second relevant parameter is the asymmetry $\chi = (P^+ - P^-)/(P^+ +$

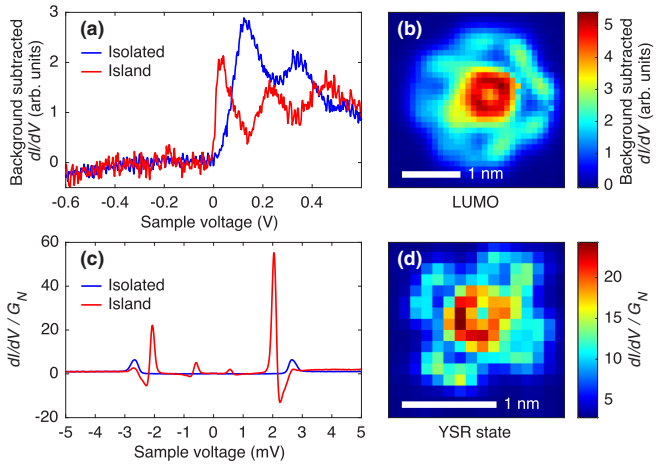


FIG. 6. (a), (c) $dI/dV$ spectra of PbPc ↑, isolated (blue curves) and inside an ordered island (red curves). In (a), a spectrum of the Pb(100) substrate was subtracted for background correction. The resonances at low voltages in (a) are attributed to the LUMO. They are located at 140 mV for the isolated molecule and at 30 mV for the molecule inside an island. Additional resonances at higher voltages are likely due to vibronic excitations. The low-bias spectra in (c) show the coherence peaks of the Pb substrate on the isolated molecule. In contrast, the spectrum measured inside an island exhibits resonances with different heights at $\approx \pm 2.05$ mV, i.e., inside the superconductor gap. The small features at $\approx \pm 0.57$ mV are replicas of these peaks due to tunneling of thermally excited electrons or holes. Temperature of the tip and the sample: 2.21 K. (b) Spatial map of the LUMO peak height at $V = 135$ mV of an isolated PbPc ↑ molecule. The map was generated from a $32 \times 32$ grid of $I(V)$ spectra by numerical derivation, background subtraction, and low-pass filtering. The data are normalized to the normal-state conductance $G_N$, which was determined from the constant differential conductance at $V < -3.5$ mV. (d) Map of the normalized YSR peak height ($V = 2.35$ mV) of a PbPc ↑ molecule inside an ordered island, generated from a $16 \times 16$ grid. Tip position frozen at (a) $V = 1$ V, $I = 100$ pA with a voltage modulation of $V_M = 14.1$ $\mathrm{mV_{PP}}$, and (c) $V = 6$ mV, $I = 100$ pA, $V_M = 113\,\mu\mathrm{V_{PP}}$.

$P^-$) of the peak heights $P^+$ and $P^-$ at positive and negative $V$. To determine the intrinsic asymmetry $\chi^*$, a background slope of the spectra at $|eV| \gg \Delta$ was determined and removed by division.

An overview of $\tilde{E}_P$ vs $\chi^*$ from many PbPc ↑ molecules is presented in Fig. 8. On the pristine substrate, $\tilde{E}_P = 1$ and $\chi^* = 0$. For isolated PbPc ↑ molecules (black symbols), we obtain essentially these two values, demonstrating the absence of YSR states. For PbPc ↑ molecules inside ordered islands, however, $\tilde{E}_P$ decreases while $\chi^*$ increases. In addition, there are distinct differences between the four groups of molecules A1, A2, B1, and B2. The strongest YSR states occur on A1 molecules, while A2 molecules show only weak signs of YSR states. Although the differences between B1 and B2 molecules are less pronounced, the latter molecules exhibit lower YSR energies.

For $H_2$Pc enneamers, DFT calculations revealed an electrostatic polarization of the molecular lobes, with the polarization being largest within the C-H bonds that point towards neighbor molecules (Fig. 9 of Ref. [14]). The dipoles in

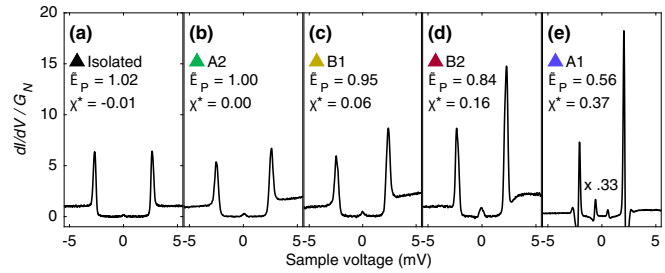


FIG. 7. $dI/dV$ spectra of PbPc ↑ molecules. (a) No YSR states are observed on isolated PbPc ↑ molecules. (b)–(e) YSR signatures of molecule classes A1 – B2. The spectrum in (e) is scaled with a factor of 0.33. All spectra were measured with the tip position frozen at $V = 6$ mV and $I = 100$ pA with $V_M = 113\,\mu\mathrm{V_{PP}}$. The parameters $\tilde{E}_P$ and $\chi^*$ are discussed in the main text.

turn electrostatically shift the molecular orbitals. We suggest that the same effect is at the origin of the different LUMO energies and YSR energies in the case of PbPc.

### C. Spatial mapping of YSR states

Figure 9 shows a spatial map of the YSR states. At the sample voltage $V = 2.6$ mV, i.e., just above the coherence peak, YSR states reduce $dI/dV$ (dark colors). The YSR states are found to be particularly pronounced on group-A1 molecules and much weaker on A2. Other molecules, such as the isolated $H_0$Pc in the upper-left corner, show increased differential conductance [yellow and red areas in Fig. 9(b)]. This effect can be attributed to the LUMO energy of the molecule, which is higher than for molecules inside the island. However, we hint that another factor may play a role. We observed that the molecules lacking a YSR state exhibit a slightly larger superconducting gap. For example, isolated PbPc ↑ molecules showed values of up to $\tilde{E}_p \approx 1.06$ (Fig. 8). An apparent

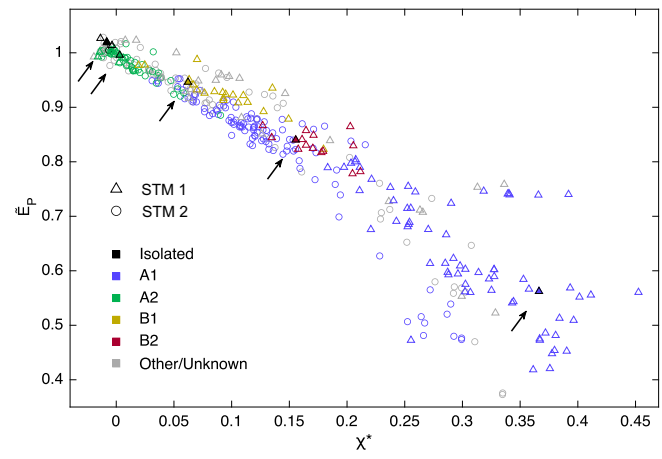


FIG. 8. $\tilde{E}_P$ vs $\chi^*$ from many PbPc ↑ molecules. Data from two STM instruments, denoted 1 and 2, are shown. Different molecular configurations are indicated by colors. Molecules of groups A1, A2, B1, and B2 were only considered when they were completely surrounded by neighbor molecules. Data points from molecules at the edges of ordered islands are labeled "Other." The spectra underlying the data points with filled symbols and arrows are shown in Fig. 7.

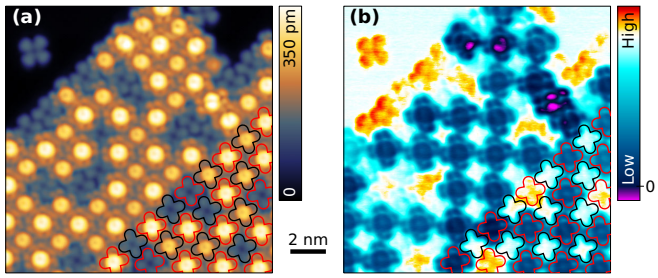


FIG. 9. (a) Topograph of a domain-A island ($V = 2.6$ mV and $I = 50$ pA). (b) $dI/dV$ map measured simultaneously with the topograph. Increased (decreased) conductance is shown in yellow and red (blue). White corresponds to the differential conductance of the substrate. YSR states reduce the differential conductance at the voltage used and thus appear blue. Negative differential conductance (purple spots) is occasionally observed. The outlines of some molecules (classes A1 and A2, in red and black, respectively) are indicated for easier comparison of the maps.

change in the superconducting gap may actually result from the two-band superconductivity of Pb [56,57]. An increased gap size shifts the coherence peak closer to the sample voltage used and thus increases the conductance.

The spatial distribution of the YSR features appears to be twofold symmetric on some of the molecules. This reduction from the fourfold symmetry of PbPc may be due to reduced symmetry of the environment, which lifts the degeneracy of the PbPc LUMO. The YSR state is then expected to be carried by the lower of the twofold-symmetric orbitals.

The presence or absence of Pb ions introduces a degree of randomness into the molecular islands, despite the regular lateral arrangement of the molecules. Similarly, Fig. 8 reveals variations of the YSR state energies among different groups of molecules but also within a single group. For example, the YSR energies in group A1 scatter between 0.4 Δ and 0.95 Δ. Below we relate this variability to differences in the shell of neighbors.

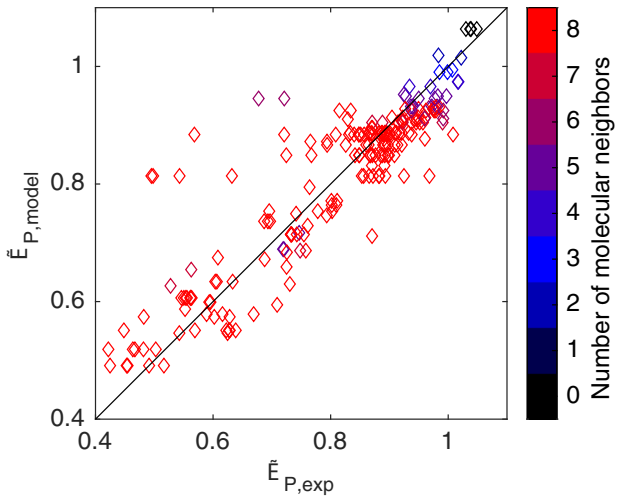


FIG. 10. Parametrization of the peak energy. Data from A1 PbPc ↑ molecules and isolated PbPc ↑ molecules are shown. The black line indicates a fit according to Eq. (1).

TABLE II. Fit of model parameters $\epsilon(t, d)$ multiplied by 1000. For an isolated molecule, the fit leads to $E_{p,0} = 1.064 \pm 0.057$. Margins represent 95% confidence intervals from the fit. NN and NNN PbPc ↓ molecules have a significant impact on the YSR energy of a PbPc ↑ molecule.

| Type | NN | NNN |
|---|---|---|
| PbPc ↑ | $-25 \pm 22$ | $-20 \pm 16$ |
| PbPc ↓ | $-102 \pm 24$ | $-48 \pm 22$ |
| $H_0$Pc | $-42 \pm 24$ | $-00 \pm 18$ |

In ordered islands consisting of PbPc ↑, PbPc ↓, and $H_0$Pc molecules, the shells of nearest and next-nearest neighbors (NN and NNN, respectively) may contain any combination of these constituents. We define a model energy

$$\tilde{E}_{P,\mathrm{model}} = \tilde{E}_{P,0} + \sum_n \epsilon(t_n, d_n), \tag{1}$$

where $\tilde{E}_{P,0}$ is a starting value. The environment introduces shifts $\epsilon(t_n, d_n)$ that depend on the type $t_n$ (PbPc ↑, PbPc ↓, or $H_0$Pc) of a neighbor and its distance $d_n$ (NN or NNN). The summation includes NN and NNN molecules.

Table II shows the results of a fit (Fig. 10) of this model to the experimental data. As expected, each additional molecular neighbor reduces the peak energy. PbPc ↓ neighbors have a large impact on the peak energy $\tilde{E}_P$, whereas the influence of PbPc ↑ and $H_0$Pc neighbors is less significant. States with the lowest $\tilde{E}_P$ of $\approx 0.4$ are observed when all NN and NNN sites are occupied by PbPc ↓ molecules.

At first glance, an antiparallel alignment of the electrostatic dipole of the central molecule with respect to the neighboring dipoles might be expected to lower the LUMO energy. However, a calculation of the effects of the electrostatic stray fields of PbPc ↑ and PbPc ↓ neighbors predicts only small differences because the main contribution to the field is due to the positive hydrogen atoms at the periphery. They electrostatically shift the LUMO of the NN molecules by 33 meV if image charges are neglected and slightly less if image charges are considered (20 and 29 meV for PbPc ↓ and PbPc ↑, respectively). These values are similar to the electrostatic shifts previously found for $H_2$Pc [14]. We speculate that the different shifts caused by PbPc ↑ and PbPc ↓ neighbors may be be related to their different LUMO energies. Since the PbPc ↑ LUMO is closer to $E_F$, a partial occupation seems likely. The corresponding negative charge is expected to counteract the effect of the positive hydrogen ions. A quantitative estimate would require additional data on the molecular geometries in the adsorbed states and the position of the image plane. In addition, a microscopic description of screening may be necessary.

## V. SUMMARY

Similar to $H_2$Pc, PbPc is diamagnetic in gas phase but becomes paramagnetic upon assembly into suitable clusters on a Pb(100) surface. This is evidenced by pronounced YSR resonances in the superconducting gap of Pb, typically at lower energies than for $H_2$Pc. The paramagnetism results from electrostatic shifts of the LUMO that are caused by induced

horizontal dipole moments in a molecule and its interacting neighbors. In particular, arrays that are disordered with respect to the up and down orientations of the PbPc molecules exhibit a range of YSR state energies. Statistical analysis is used to quantify the influence of nearest- and next-nearest-neighbor molecules. The interaction of the charge distribution of the PbPc molecules with its image charge leads to a shift between the orbitals of PbPc ↑ and PbPc ↓ molecules.

To date, three phthalocyanines have been found to exhibit electrostatically induced paramagnetism on a substrate. Their common features are a LUMO that is quite close to the Fermi level and a heterocycle that provides partial charges for intermolecular electrostatic interaction. These requirements are likely to be met by a number of closed-shell molecules, which may be made paramagnetic on substrates.


[1] V. Meded, A. Bagrets, K. Fink, R. Chandrasekar, M. Ruben, F. Evers, A. Bernand-Mantel, J. S. Seldenthuis, A. Beukman, and H. S. J. van der Zant, Electrical control over the Fe(II) spin crossover in a single molecule: Theory and experiment, Phys. Rev. B **83**, 245415 (2011).

[2] M. Gruber and R. Berndt, Spin-crossover complexes in direct contact with surfaces, Magnetochemistry **6**, 35 (2020).

[3] S. Yazdani, J. Phillips, T. K. Ekanayaka, R. Cheng, and P. A. Dowben, The influence of the substrate on the functionality of spin crossover molecular materials, Molecules **28**, 3735 (2023).

[4] Y. Zhao, K. Jiang, C. Li, Y. Liu, C. Xu, W. Zheng, D. Guan, Y. Li, H. Zheng, C. Liu, W. Luo, J. Jia, X. Zhuang, and S. Wang, Precise control of $\pi$-electron magnetism in metal-free porphyrins, J. Am. Chem. Soc. **142**, 18532 (2020).

[5] T. Wang, A. Berdonces-Layunta, N. Friedrich, M. Vilas-Varela, J. P. Calupitan, J. I. Pascual, D. Peña, D. Casanova, M. Corso, and D. G. de Oteyza, Aza-triangulene: On-surface synthesis and electronic and magnetic properties, J. Am. Chem. Soc. **144**, 4522 (2022).

[6] S. Karan, N. Li, Y. Zhang, Y. He, I. P. Hong, H. Song, J.-T. Lü, Y. Wang, L. Peng, K. Wu, G. S. Michelitsch, R. J. Maurer, K. Diller, K. Reuter, A. Weismann, and R. Berndt, Spin manipulation by creation of single-molecule radical cations, Phys. Rev. Lett. **116**, 027201 (2016).

[7] M.-L. Bocquet, N. Lorente, R. Berndt, and M. Gruber, Spin in a closed-shell organic molecule on a metal substrate generated by a sigmatropic reaction, Angew. Chem. Int. Ed. **58**, 821 (2019).

[8] T. G. Gopakumar, F. Matino, H. Naggert, A. Bannwarth, F. Tuczek, and R. Berndt, Electron-induced spin crossover of single molecules in a bilayer on gold, Angew. Chem. Int. Ed. **51**, 6262 (2012).

[9] T. Miyamachi, M. Gruber, V. Davesne, M. Bowen, S. Boukari, L. Joly, F. Scheurer, G. Rogez, T. K. Yamada, P. Ohresser, E. Beaurepaire, and W. Wulfhekel, Robust spin crossover and memristance across a single molecule, Nat. Commun. **3**, 938 (2012).

[10] L. Malavolti, M. Briganti, M. Hänze, G. Serrano, I. Cimatti, G. McMurtrie, E. Otero, P. Ohresser, F. Totti, M. Mannini, R. Sessoli, and S. Loth, Tunable spin–superconductor coupling of spin 1/2 vanadyl phthalocyanine molecules, Nano Lett. **18**, 7955 (2018).

[11] C. Fourmental, S. Mondal, R. Banerjee, A. Bellec, Y. Garreau, A. Coati, C. Chacon, Y. Girard, J. Lagoute, S. Rousset, M.-L. Boillot, T. Mallah, C. Enachescu, C. Barreteau, Y. J. Dappe, A. Smogunov, S. Narasimhan, and V. Repain, Importance of epitaxial strain at a spin-crossover molecule–metal interface, J. Phys. Chem. Lett. **10**, 4103 (2019).

[12] J. Liu, Y. Gao, T. Wang, Q. Xue, M. Hua, Y. Wang, L. Huang, and N. Lin, Collective spin manipulation in antiferroelastic spin-crossover metallo-supramolecular chains, ACS Nano **14**, 11283 (2020).

[13] S. Johannsen, S. Ossinger, T. Markussen, F. Tuczek, M. Gruber, and R. Berndt, Electron-induced spin-crossover in self-assembled tetramers, ACS Nano **15**, 11770 (2021).

[14] J. Homberg, A. Weismann, R. Berndt, and M. Gruber, Inducing and controlling molecular magnetism through supramolecular manipulation, ACS Nano **14**, 17387 (2020).

[15] C. Li, J. Homberg, A. Weismann, and R. Berndt, On-surface synthesis and spectroscopy of aluminum phthalocyanine on superconducting lead, ACS Nano **16**, 16987 (2022).

[16] Yu luh, Bound state in superconductors with paramagnetic impurities, Acta Phys. Sin. **21**, 75 (1965).

[17] H. Shiba, Classical spins in superconductors, Prog. Theor. Phys. **40**, 435 (1968).

[18] A. I. Rusinov, On the theory of gapless superconductivity in alloys containing paramagnetic impurities, Zh. Eksp. Teor. Fiz. **56**, 2047 (1969) [Sov. Phys.-JETP **29**, 1101 (1969)].

[19] A. Yazdani, B. A. Jones, C. P. Lutz, M. F. Crommie, and D. M. Eigler, Probing the local effects of magnetic impurities on superconductivity, Science **275**, 1767 (1997).

[20] K. J. Franke, G. Schulze, and J. I. Pascual, Competition of superconducting phenomena and Kondo screening at the nanoscale, Science **332**, 940 (2011).

[21] N. Hatter, B. W. Heinrich, D. Rolf, and K. J. Franke, Scaling of Yu-Shiba-Rusinov energies in the weak-coupling Kondo regime, Nat. Commun. **8**, 2016 (2017).

[22] B. W. Heinrich, J. I. Pascual, and K. J. Franke, Single magnetic adsorbates on s-wave superconductors, Prog. Surf. Sci. **93**, 1 (2018).

[23] J. Brand, S. Gozdzik, N. Néel, J. L. Lado, J. Fernández-Rossier, and J. Kröger, Electron and Cooper-pair transport across a single magnetic molecule explored with a scanning tunneling microscope, Phys. Rev. B **97**, 195429 (2018).

[24] S. Kezilebieke, M. Dvorak, T. Ojanen, and P. Liljeroth, Coupled Yu-Shiba-Rusinov states in molecular dimers on $NbSe_2$, Nano Lett. **18**, 2311 (2018).

[25] S. Kezilebieke, R. Žitko, M. Dvorak, T. Ojanen, and P. Liljeroth, Observation of coexistence of Yu-Shiba-Rusinov states and spin-flip excitations, Nano Lett. **19**, 4614 (2019).

[26] S. Lu, H. Nam, P. Xiao, M. Liu, Y. Guo, Y. Bai, Z. Cheng, J. Deng, Y. Li, H. Zhou, G. Henkelman, G. A. Fiete, H.-J. Gao, A. H. MacDonald, C. Zhang, and C.-K. Shih, PTCDA molecular monolayer on Pb thin films: An unusual electron Kondo system and its interplay with a quantum-confined superconductor, Phys. Rev. Lett. **127**, 186805 (2021).

[27] C. Rubio-Verdú, J. Zaldívar, R. Žitko, and J. I. Pascual, Coupled Yu-Shiba-Rusinov states induced by a many-body molecular spin on a superconductor, Phys. Rev. Lett. **126**, 017001 (2021).

[28] S. M. F. Shahed, F. Ara, M. I. Hossain, K. Katoh, M. Yamashita, and T. Komeda, Observation of Yu-Shiba-Rusinov states and inelastic tunneling spectroscopy for intramolecule magnetic exchange interaction energy of terbium phthalocyanine (TbPc) species adsorbed on superconductor $NbSe_2$, ACS Nano **16**, 7651 (2022).

[29] K. Vaxevani, J. Li, S. Trivini, J. Ortuzar, D. Longo, D. Wang, and J. I. Pascual, Extending the spin excitation lifetime of a magnetic molecule on a proximitized superconductor, Nano Lett. **22**, 6075 (2022).

[30] J. Homberg, A. Weismann, T. Markussen, and R. Berndt, Resonance-enhanced vibrational spectroscopy of molecules on a superconductor, Phys. Rev. Lett. **129**, 116801 (2022).

[31] J. Homberg, M. Gruber, A. Weismann, and R. Berndt, Enhanced conductance of molecular states at interstitial sites, New J. Phys. **25**, 013029 (2023).

[32] S. Trivini, J. Ortuzar, K. Vaxevani, J. Li, F. S. Bergeret, M. A. Cazalilla, and J. I. Pascual, Cooper pair excitation mediated by a molecular quantum spin on a superconducting proximitized gold film, Phys. Rev. Lett. **130**, 136004 (2023).

[33] S. Nadj-Perge, I. K. Drozdov, B. A. Bernevig, and A. Yazdani, Proposal for realizing Majorana fermions in chains of magnetic atoms on a superconductor, Phys. Rev. B **88**, 020407(R) (2013).

[34] S. Jeon, Y. Xie, J. Li, Z. Wang, B. A. Bernevig, and A. Yazdani, Distinguishing a Majorana zero mode using spin-resolved measurements, Science **358**, 772 (2017).

[35] H. Kim, A. Palacio-Morales, T. Posske, L. Rózsa, K. Palotás, L. Szunyogh, M. Thorwart, and R. Wiesendanger, Toward tailoring Majorana bound states in artificially constructed magnetic atom chains on elemental superconductors, Sci. Adv. **4**, eaar5251 (2018).

[36] J. F. Steiner, C. Mora, K. J. Franke, and F. von Oppen, Quantum magnetism and topological superconductivity in Yu-Shiba-Rusinov chains, Phys. Rev. Lett. **128**, 036801 (2022).

[37] Y. F. Wang, J. Kröger, R. Berndt, H. Vázquez, M. Brandbyge, and M. Paulsson, Atomic-scale control of electron transport through single molecules, Phys. Rev. Lett. **104**, 176802 (2010).

[38] A. Gerlach, T. Hosokai, S. Duhm, S. Kera, O. T. Hofmann, E. Zojer, J. Zegenhagen, and F. Schreiber, Orientational ordering of nonplanar phthalocyanines on Cu(111): Strength and orientation of the electric dipole moment, Phys. Rev. Lett. **106**, 156102 (2011).

[39] B. Yuan, P. Chen, J. Zhang, Z. Cheng, X. Qiu, and C. Wang, Orientation of molecular interface dipole on metal surface investigated by noncontact atomic force microscopy, Chin. Sci. Bull. **58**, 3630 (2013).

[40] Y. L. Huang, W. Chen, F. Bussolotti, T. C. Niu, A. T. S. Wee, N. Ueno, and S. Kera, Impact of molecule-dipole orientation on energy level alignment at the submolecular scale, Phys. Rev. B **87**, 085205 (2013).

[41] M. Lackinger and M. Hietschold, Determining adsorption geometry of individual tin-phthalocyanine molecules on Ag(111) – A STM study at submonolayer coverage, Surf. Sci. **520**, L619 (2002).

[42] C. Stadler, S. Hansen, F. Pollinger, C. Kumpf, E. Umbach, T.-L. Lee, and J. Zegenhagen, Structural investigation of the adsorption of SnPc on Ag(111) using normal-incidence x-ray standing waves, Phys. Rev. B **74**, 035404 (2006).

[43] R. Woolley, C. Martin, G. Miller, V. Dhanak, and P. Moriarty, Adsorbed molecular shuttlecocks: An NIXSW study of Sn phthalocyanine on Ag(111) using Auger electron detection, Surf. Sci. **601**, 1231 (2007).

[44] Y. Wang, J. Kröger, R. Berndt, and W. Hofer, Structural and electronic properties of ultrathin tin-phthalocyanine films on Ag(111) at the single-molecule level, Angew Chem. Int. Ed. **48**, 1261 (2009).

[45] Y. Wang, J. Kröger, R. Berndt, and W. A. Hofer, Pushing and pulling a Sn ion through an adsorbed phthalocyanine molecule, J. Am. Chem. Soc. **131**, 3639 (2009).

[46] A. Sperl, J. Kröger, and R. Berndt, Demetalation of a single organometallic complex, J. Am. Chem. Soc. **133**, 11007 (2011).

[47] A. Sperl, J. Kröger, and R. Berndt, Controlled metalation of a single adsorbed phthalocyanine, Angew. Chem. **123**, 5406 (2011).

[48] I. Kröger, B. Stadtmüller, C. Kleimann, P. Rajput, and C. Kumpf, Normal-incidence x-ray standing-wave study of copper phthalocyanine submonolayers on Cu(111) and Au(111), Phys. Rev. B **83**, 195414 (2011).

[49] M. Ziegler, N. Néel, A. Sperl, J. Kröger, and R. Berndt, Local density of states from constant-current tunneling spectra, Phys. Rev. B **80**, 125402 (2009).

[50] J. D. Baran, J. A. Larsson, R. A. J. Woolley, Y. Cong, P. J. Moriarty, A. A. Cafolla, K. Schulte, and V. R. Dhanak, Theoretical and experimental comparison of SnPc, PbPc, and CoPc adsorption on Ag(111), Phys. Rev. B **81**, 075413 (2010).

[51] A. Lee, D. Kim, S.-H. Choi, J.-W. Park, J.-Y. Jaung, and D. Jung, Theoretical study on phthalocyanine, pyrazinoporphyrazine and their complexation with $Mg^{2+}$ and $Zn^{2+}$, Mol. Simulat. **36**, 192 (2010).

[52] P. Järvinen, S. K. Hämäläinen, M. Ijäs, A. Harju, and P. Liljeroth, Self-assembly and orbital imaging of metal phthalocyanines on a graphene model surface, J. Phys. Chem. C **118**, 13320 (2014).

[53] J. E. Griffith and G. P. Kochanski, Scanning tunneling microscopy, Annu. Rev. Mater. Sci. **20**, 219 (1990).

[54] T. Klitsner, R. S. Becker, and J. S. Vickers, Observation of the effect of tip electronic states on tunnel spectra acquired with the scanning tunneling microscope, Phys. Rev. B **41**, 3837 (1990).

[55] This range of $E_{\mathrm{YSR}}$ values corresponds to voltages between approximately 1.4 and 2 $\Delta/e$ in the conductance spectra.

[56] M. Ruby, B. W. Heinrich, J. I. Pascual, and K. J. Franke, Experimental demonstration of a two-band superconducting state for lead using scanning tunneling spectroscopy, Phys. Rev. Lett. **114**, 157001 (2015).

[57] T. Gozlinski, Q. Li, R. Heid, R. Nemoto, R. Willa, T. K. Yamada, J. Schmalian, and W. Wulfhekel, Band-resolved Caroli–de Gennes–Matricon states of multiple-flux-quanta vortices in a multiband superconductor, Sci. Adv. **9**, eadh9163 (2023).

*Correction:* A misspelled word appeared in the title and twice in Sec. I and has been fixed.